

This is the peer-reviewed version of the article:

Goran M. Stojanović, Jasmina Nikodinović-Runić, Stefan Švenderman, Tijana Kojić, Milan Radovanović, Momir Mikovc, Danijela Randjelović, Comprehensive characterization of elastomeric polyhydroxyalkanoate and its sensor applications, Materials Science & Engineering C, 2020, 115, 111091, <https://doi.org/10.1016/j.msec.2020.111091>



This work is licensed under the [Attribution-NonCommercial-NoDerivatives 4.0 International \(CC BY-NC-ND 4.0\)](https://creativecommons.org/licenses/by-nc-nd/4.0/)

1 Title page:
2
3
4
5

6 Comprehensive characterization of elastomeric Polyhydroxyalkanoate and its sensor
7 applications
8
9

10
11 Goran Stojanović^a, Jasmina Nikodinović-Runić^b, Stefan Švenderman^a, Tijana Kojić^{a,*}, Milan
12 Radovanović^a, Momir Mikov^c, Danijela Ranđelović^d
13
14
15

16 ^aFaculty of Technical Sciences, University of Novi Sad, Trg Dositeja Obradovića 6, 21000 Novi Sad, Serbia

17 ^bInstitute of Molecular Genetics and Genetic Engineering, University of Belgrade, Vojvode Stepe 444a,
18 11000 Belgrade, Serbia

19 ^cFaculty of Medicine, University of Novi Sad, Hajduk Veljkova 3, 21000 Novi Sad, Serbia

20 ^dDepartment of Microelectronic Technologies, Institute of Chemistry, Technology and Metallurgy, University
21 of Belgrade, Njegoševa 12, 11000 Belgrade, Serbia
22
23
24
25
26
27
28
29
30
31
32
33
34
35
36
37
38
39
40
41
42
43

44 1. Introduction

45 More than 320 million tons of plastics generated per year represent a serious environmental problem
46 and potential hazard [1]. Biopolymers, particularly polyhydroxyalkanoates (PHAs), are promising
47 alternatives to a slow- or nondegradable petroleum-based plastics [2]. PHAs are biopolyesters that have
48 been applied in many sectors of modern science and industry. PHAs are biocompatible and
49 biodegradable and as such have a positive social and environmental dimension [3]. Degradation
50 metabolites of PHAs are not toxic; they degrade into carbon dioxide and water (under aerobic
51 conditions), or carbon dioxide and methane (under anaerobic conditions) [4]. In 2007, the Food and
52 Drug Administration (FDA) approved the use of P(4HB) for surgical sutures in clinical applications
53 and from that period medical applications of PHAs have increased [5]. Examples of these applications
54 include: scaffold for heart valve and cartilage tissue, micro- and nanospheres and antibacterial coating
55 material [6], [7]. PHAs are mainly produced by biotechnological (fermentative) methods. More than
56 150 PHA subunits have been identified to date [8] and their structure determines mechanical properties
57 and degradation rate [9]. PHAs can be degraded by the activity of microorganisms (bacteria and fungi),
58 but also by enzymes in bovine serum, pancreatin and synthetic gastric juice [10]. The carbon sources
59 and the metabolic potential of the microorganisms involved in their synthesis have an influence on PHA
60 chemical properties [11]. The molecular mass of PHA is dependent on growth conditions such as carbon
61 source, culture medium or fermentation mode [12]. PHAs are insoluble in water, but soluble in
62 chloroform and demonstrated a good resistance to moisture and UV light [13]. The composition of the
63 monomeric unit of PHAs has an influence on their mechanical and temperature characteristics with
64 short chain length (scl) PHAs being hard, brittle polymers while medium chain length (mcl) PHAs are
65 softer, more elastomeric polymers [14]. The mechanical properties of PHAs can be improved by means
66 of an electrospinning technique [15]. Combining PHAs with other polymers can improve their
67 flexibility, which is an important parameter for medical applications [16]. The melting temperature of
68 scl-PHA is above 140°C, while melting temperatures of mcl-PHA is usually between 40 and 60°C, and
69 above this range they are amorphous and sticky. However, melting temperatures are highly dependent
70 on the monomer composition, thus mcl-PHA homopolymers can have melting temperatures even higher
71 than 60°C [16, 17]. The applications of PHAs as biodegradable polymers is manifold and it will be even
72 higher if their mechanical and hydrophobic properties can be modified and fine-tuned with respect to
73 the requirements of the specific application [18]. Aligning fibers in the internal structure of PHA,
74 achieved by the electrospinning technique, can improve the mechanical characteristics compared with
75 randomly oriented fibers inside the PHA structure [19]. Furthermore, the wettability and the contact
76 angle of polyhydroxyalkanoates electrospun membranes can also be adjusted by changing the polymer
77 concentration [20].

78 An analysis of the literature reveals that the majority of published papers have considered (bio)medical
79 applications of PHAs, but there is a lack of articles reporting sensor applications of PHAs. Previously,
80 PHB film was reported to be suitable as a membrane for the incorporation of haemoglobin to boost the
81 electron transfer rate of this protein. Further modifications using pyrolytic graphite electrodes and/or
82 the addition of peroxidases paved the way towards the application of PHB-embedded proteins as an
83 integral part of H₂O₂ biosensors [21], [22]. Only one more biosensor application was found in the
84 literature; another type of PHA (biopolymer containing 3-hydroxyvalerate (3HV), 5-hydroxydecenoate
85 (5HDE) and 3-hydroxyoctadecenoate (3HODE)) was used to develop of a hybrid nanocomposite based
86 biosensor containing gold nanoparticles, horse radish peroxidase and PHA/AuNP/HRP/ITO for the
87 quantitative detection of artemisinin in body fluids [23].

88 This study aims to expand the application niche of PHA based sensors. Herein we analyse the structural,
89 morphological and mechanical properties of a biotechnologically produced PHA sample, more
90 specifically a medium chain length PHA (mcl-PHA). The inductive-capacitive (LC) resonant circuit
91 structure was constructed using this sample. This device was applied for the remote detection of liquid
92 solution in which the sensor was immersed (such as artificial saliva or simulated gastric fluid). Using

93 the principles of wireless coupling we have successfully detected the chosen fluid by measuring the
94 shift in the resonant frequency of the LC structure fabricated on a PHA substrate covered with gold as
95 a conductive material.

96

97 **2. Materials and Methods**

98 *2.1 Production method of PHA sample*

99 Mcl-PHA biopolymer, specifically polyhydroxyoctanoate (PHO; contained > 95% 3-hydroxyoctanoic
100 acid as the monomer), was produced via fermentation using *Pseudomonas putida* KT2440 strain by
101 Bioplastech Ltd., using basic fermentation conditions as described previously [24] and the octanoic acid
102 as substrate [25]. The PHO content of cells was determined by methanolysis of 10 to 15 mg of
103 lyophilized cells in the presence of 15% (vol/vol) sulfuric acid. The resulting methyl esters of the
104 constituent hydroxyalkanoic acids were analyzed by gas chromatography. For identification of the
105 methylesters, gas chromatography-tandem mass spectrometry (GC-MS-MS) was also performed. The
106 remaining monomers were trace amounts of 3-hydroxyhexanoate and 3-hydroxydecanoate. Mcl-PHA
107 films were prepared by the solvent casting method. Initially, PHA (2 g) was dissolved in acetone (10
108 mL) at 25 °C, after which it was poured into a glass Petri dish and left to dry in the air at ambient
109 temperature for 10 days.

110 *2.2 Characterization methods*

111 A 3D optical Profilometer (Huvitz microscope with Panasis software) and scanning electron
112 microscopy (SEM, Hitachi TM3030) were used for structural and surface analysis. Morphology,
113 roughness and frictional properties of the sample were studied with an atomic force microscope
114 AutoProbe CP-Research SPM (TM Microscopes-Bruker) using a 90 µm large area scanner. The
115 measurements were performed in contact mode using Bruker Phosphorous (n)-doped silicon contact
116 metrology probes, model MPP-31123-10 with Al reflective coating and symmetric tip. AFM images of
117 topography, “error signal” and Lateral Force Microscopy (LFM) signal were taken and later analyzed
118 using two software packages, Image Processing and Data Analysis Version 2.1.15 and SPMLab
119 Analysis, DI SPMLab NT Ver. 6.0.2. The contact angle method was used for wettability analysis. The
120 contact angle measurement was performed in an optical laboratory located in a clean room class ISO 8,
121 nitrogen and air class ISO 5, vacuum. A Bausch & Lomb MicroZoom Microscope connected to a laptop
122 with software tool ISCapture were used for photography. Laboratory Power Supply Manson NSP 3630
123 provided the necessary light for measurement. For mechanical characterization, a nanoindentation
124 method was used with a G200 nanoindenter, having a Berkovich diamond tip. A Vector Network
125 Analyzer E5071B was used for measuring S-parameters of LC structure, in different media.

126 *2.3 Preparation of test fluids*

127 Two different fluids were prepared in order to test functionality of the fabricated structure: (a) artificial
128 saliva and (b) simulated gastric fluid. The artificial saliva had the following composition: Sodium
129 carboxymethylcellulose – 10 g/l, Sorbitol – 29.95 g/l, Methyl p-hydroxybenzoate – 1.00 g/l, Sodium
130 chloride – 0.87 g/l, Di-potassium hydrogen orthophosphate – 0.80 g/l, Potassium chloride – 0.22 g/l and
131 Lemon aroma – 5 ml. The simulated gastric fluid, without pepsin, was prepared as mixture of 0.2%
132 (w/v) Sodium Chloride in 0.7% (v/v) Hydrochloric Acid adjusted to pH equal to 1.2 [26].

133

134 **3. Results and Discussion**

135 *3.1 Structural, morphological and wettability properties of PHA sample*

136 *3.1.1. Structural characterization*

137 In the last few years, PHAs have been studied to be used in tissue engineering for hard and soft tissue
138 replacement, and as therapeutic delivery carriers [27]. For such applications mostly scl-PHAs, such as
139 polyhydroxybutyrate (PHB) and its copolymers have been applied.

140 In this study, polyhydroxyoctanoate (PHO), representative of the mcl-PHA family, was evaluated for
141 biosensor applications due to its specific thermo-elastomeric characteristics. Processed mcl-PHA film
142 sample is shown in Fig. 1(a). Structural characterization was performed by SEM to visualise the surface
143 and the cross section of the PHA sample. An SEM micrograph of the polymer surface with a
144 magnification of 200 is presented in Fig. 1(b), while a cross section of the sample with magnification
145 of 250 times is depicted in Fig. 1(c). Speckles of dust are evident on the surface of the film (Fig. 1(b))
146 while the side of the film that was in contact with glass during the solvent casting appears denser, as
147 the cross section revealed (Fig. 1(c)).

148
149

Figure 1.

150

151 A 3D Optical profilometer was used to determine the exact thickness of the PHA polymer. The role of
152 the profilometer was to provide 2D and 3D insight into topographic surfaces, and was used for micro-
153 and nano-level measurements. Due to the transparency of the sample, the surface of the polymer was
154 coloured purple with a marker, prior to starting measurement with the 3D Profilometer. The purple dye
155 did not affect the measurement parameters or the performance of the device. The 2D image obtained is
156 presented in Fig. 2(a) with magnification of $\times 20$, and the 3D image is presented in Fig. 2(b). The 3D
157 profile shows the thickness of the sample, which was estimated to be around $300 \mu\text{m}$. The polymer was
158 not of uniform thickness across the whole surface, and varied in the range $\pm 10 \mu\text{m}$.

159

160

Figure 2.

161

162 *3.1.2. Morphological characterization*

163 Selected results of AFM characterization are presented in Figs. 3 and 4. The 3D topography of the
164 sample is shown in Fig. 3 for the two scanning areas, (a) $50 \mu\text{m} \times 50 \mu\text{m}$, and (b) $5 \mu\text{m} \times 5 \mu\text{m}$. For
165 these areas, RMS roughness of the sample was 608 nm and 73 nm, respectively. Results of LFM
166 measurements are shown in Fig. 4. For the mentioned scanning areas, topography and LFM images are
167 shown in parallel. By analyzing these images we can conclude that the sample surface is heterogeneous
168 regarding frictional properties. The darker the region on the LFM image, the higher the value of the
169 friction coefficient. In other words, the darker regions are “stickier” than the rest of the sample.

170

171

Figure 3.

172

173

Figure 4.

174

175 PHA films or membranes can be produced by various techniques that include compression-molding,
176 solvent-casting, or electrospinning, and more recently 3D printing fabrication [28]. It has been shown
177 previously that solvent-casted films have higher roughness in comparison to the compression-molded
178 PHA membranes, however that did not affect the adherence of cerebellar granule neurons [29].

179 *3.1.3. Characterization of wettability*

180 For this purpose, we used the contact angle method where the static contact angle of a droplet on a
181 polymer was measured over a period of time until the droplet (about 2 μl) was absorbed or spilled over
182 the surface. The droplet images were analyzed by ImageJ software (option *drop_analysis*) depicted in
183 Fig. 5.

184 *Figure 5.*

185 Fig. 5(b) illustrates the change of contact angle for a drop of distilled water over a period of 10 minutes.
186 The values of the contact angle over the entire measurement period, to which the polymer was subjected,
187 are below 90° , which categorize this polymer as hydrophilic, which means with higher wettability. An
188 increase in the number of polar groups can make polymers more hydrophilic. This property is favorable
189 for PHA sensor applications such as the LC sensor described in this paper, because it ensures that the
190 liquid medium has better contact with the substrate.
191

192 *3.2 Mechanical properties of PHA sample*

193 One of the most important material properties is its mechanical endurance, which shows how much load
194 (force, moment) a structure fabricated of the specific material can resist. Multiple nanoindentation tests
195 were carried out with sets of ten indentations to ensure the credibility of the measured results. A preset
196 depth of 5 μm was set, while the reaching load time was set to 15 s, and the peak loading time was set
197 to 5 s. Nanoindentation testing was performed in three cases: (1) PHA sample; (2) PHA sample after
198 incubation in artificial saliva for twenty-four hours, and (3) PHA sample after immersing in a simulated
199 gastric fluid for twenty-four hours. The results obtained are depicted in Fig. 6.

200 *Figure 6.*

201 Fig. 6 shows the mean load–displacement curves for a maximum preset depth of 5 μm , where the
202 penetration loads were around 2.7 mN for pure PHA, 2.5 mN for the polymer in saliva, and 2 mN for
203 the polymer in gastric acid. It can be seen from Fig. 6 that the displacement into the surface exceeds the
204 preset depth of 5 μm by a few nanometers, due to the hold time of 5 s on the preset depth so the tip
205 enters a few nanometers more into the studied material. The obtained results confirmed theoretical
206 expectations; the pure polymer demonstrated the highest resistance to mechanical stress. When the
207 polymer was in saliva, this fluid reduced its mechanical properties, softening the material. The polymer
208 that was immersed in the gastric fluid exhibited the lowest resistance to mechanical force. This is due
209 to gastric fluid being an acid with pH around 1.2, which leads to degradation of the polymer and the
210 breaking of double bonds within the polymer structure. The measured values of Young’s modulus were
211 58.8 MPa in the case of pure PHA sample, 49.1 MPa for PHA in the artificial saliva and 38.1 MPa for
212 PHA in the gastric fluid, respectively. The hardness value was 8 MPa for the PHA sample, 7 MPa for
213 PHA in the artificial saliva and 5 MPa for PHA in the gastric fluid. These differences in elastic modulus
214 and hardness values are a consequence of the exposure of the PHA sample to fluids that affected its
215 elasticity and strength. The obtained values of the studied parameters are in good agreement with the
216 data available in the literature. In [30] Young’s modulus had a maximum of 25.4, 14.1, and 12.6 MPa
217 for polyhydroxyoctanoate (PHO) films obtained from ethyl acetate, acetone, and chloroform solution,
218 respectively. These values are comparable with the values for Young’s modulus presented in our study,
219 however, in [30], authors used an additional step for PHO film purification, which is one of the reason
220 to consider our approach more eco-friendly. In our study, the ratio “displacement/thickness of the PHA
221 film” was very low (around 0.016), meaning that nanoindentation tip will reach only the superficial
222 layer of PHA. However, a thinner polymer film will have higher Young’s modulus values, more
223 precisely higher values of displacement/thickness ratio will result in an increase of Young’s modulus,
224 which is caused by the substrate effect.

225 Since the sensor proved to be a fully functional device, several material characterization methods were
226 applied in order to assess the quality of the solvent-casted mcl-PHA film itself as well as to analyse
227 structural, morphological, mechanical and wettability properties, which are essential for the underlying
228 operation principle and field of application of the sensor. SEM analysis was used to detect density of
229 the polymer as a substrate of the developed sensor. 3D profilometer was used to determine the thickness
230 of the substrate, because sensor properties are dependent on this thickness. AFM analysis was
231 implemented to determine the roughness of used PHA film, because this surface property influences
232 how applied material or media will have a good adherence on the surface of the structure. Most
233 biosensor applications for PHA polymers would be within a liquid environment, thus wettability was
234 also studied. One of the intended applications of the proposed structure is in the field of the self-
235 degradable sensors in the media in our body. Because of that, we also analyzed mechanical properties
236 or how the presented sensor softens up when exposed to saliva or gastric fluid.

237

238 *3.3 Sensor applications*

239 We designed an inductor-capacitor (LC) structure, composed of an interdigitated capacitor with 5 pairs
240 of fingers (electrodes) and a helically wound inductor. Uniquely, both parts (components) are planar
241 and realized in one layer, which means there is no overpass or underpass such as would usually be used
242 in spiral inductor design. The width of the electrodes and the gap between them were both equal to 600
243 μm . The total dimension of the LC structure was 30 mm \times 12 mm. The LC sensor was fabricated using
244 a cutting plotter machine, curving the structure in the PHA substrate (Fig. 7(a)). After that, gold was
245 vaped onto this structure, as can be seen in Fig. 7(b), in order to obtain the conductive structure at the
246 top. Nominal capacitance of the inderdigitated part of the structure was around 10.76 pF, whereas the
247 inductance of the inductive part of the structure was approximately 1.53 nH.

248 Figure 7.

249 The Vector Network Analyzer (VNA) was used to measure the electrical characteristics of the sensor
250 as it is depicted in Fig. 8, using a copper antenna coil.

251

252 Figure 8.

253 The S11-parameter of the antenna was measured using VNA and it was subtracted from the measured
254 value of the S11-parameter obtained for the PHA-based LC structure exposed to different media. This
255 eliminated any error introduced by the antenna itself. The first measurement was conducted under
256 conditions such that the air was the dielectric material between the fingers of the interdigitated capacitor.
257 The second and third measurement cycles were performed with artificial saliva or artificial gastric fluid,
258 respectively, between the electrodes of the capacitor. The measured amplitude of the S11-parameter as
259 a function of frequency is presented in Fig. 9, for the three above-mentioned media.

260

261 Figure 9.

262 It can be concluded from Fig. 9, that not only a shift in the resonant frequency was obtained when the
263 sensor was exposed to different media, but also the magnitude of the S11 parameter increased in the
264 liquid medium. The sensitivity of the proposed sensors can be expressed by $\Delta S_{11}/\Delta f_{\text{res}}$ and the value of
265 0.3 dB/MHz was obtained. Figure 10 demonstrates a shift in the resonant frequency of LC structure
266 towards lower values. The value and change in the resonant frequency is determined by the type of
267 dielectric located between the fingers of the interdigitated capacitor of the LC resonant circuit structure.
268 Depending on the value of the relative permittivity of the material placed between the capacitor

269 electrodes, the capacitance of the capacitor in the LC structure varies. Capacitance has the lowest value
 270 in air while it increases after exposure to the artificial saliva, and even more after immersion in the
 271 artificial stomach acid. The resonant frequency is inversely proportional to this capacitance, based on
 272 the equation $f_{res} = 1/2 \cdot \pi \sqrt{L \cdot C}$. The studied media, artificial saliva and simulated gastric juice, have some
 273 similarities (containing water, mucus, salt), but also some differences (presence of iodide, pertechnetate,
 274 and bromide). These differences lead to different values of their relative permittivity. The difference in
 275 the dielectric constant was used to change capacitance of the capacitive part of the proposed sensor
 276 structure and consequently its resonant frequency. By means of the antenna coil, this shift in the
 277 resonant frequency can be monitored remotely, without contamination of the analysed media.
 278 Measuring S-parameters, using Vector Network Analyzer E5071B, we can determine both amplitude
 279 of S11-parameter and f_{res} in different media. This instrument was chosen as it enabled application of
 280 wireless (using antenna) and non-contact measuring principles. The qualitative advantages of this
 281 approach are as follows: (a) the terminals (wires) are not necessary from the component under test; (b)
 282 the contamination effects are eliminated; (c) the applied method is non-destructive for the tested
 283 component.

284 Figure 10.

285 Figs. 9 and 10 demonstrate that the highest resonant frequency value of the studied PHA-based LC
 286 structure was reached in air, being equal to 1.24 GHz. Resonant frequency drops to 1.23 GHz when the
 287 artificial saliva was used as the dielectric. The lowest value of the resonant frequency in the LC structure
 288 was observed when artificial gastric fluid was used as the dielectric, being equal to 1.22 GHz. Thus, a
 289 shift in the resonant frequency of 10 MHz per new medium was obtained, which can be also used as a
 290 measurable indicator of the sensitivity of the proposed structure. To compare the sensitivity of the
 291 proposed PHA-based sensor and other type of sensors from literature that also used resonant frequency
 292 as a measured quantity, Table 1 summarizes a comparison among different studies dealing with sensors
 293 for detection of various parameters of the human body. From Table 1, quantitative benefits of the
 294 proposed technique can be also noticed, because the difference in S11 amplitude and shift of resonant
 295 frequency between the various media has high values (1 dB/5 dB and 10 MHz, respectively), which
 296 enables clear distinction between them.

297 **Table 1**

298 Comparison of the sensitivity of sensors proposed in this paper and other reported studies.

Paper	Detection parameter	Sensing principle	Sensitivity (shift in)	
			Resonant freq.	Amplitude S11
This work	saliva, gastric fluid	wireless LC	10 MHz per new medium	1 dB for saliva 5 dB for gastric fl.
Ref. [31]	gastric pressure	inductive coupling LC	0.6 kHz / mmHg	n.a.
Ref. [32]	pH of liquid sample	planar inductor	4 MHz / pH	n.a.
Ref. [33]	glucose, galactose, fructose	capacitive coupling split rings	304 kHz, 540 kHz, 2.2 MHz / mg/dl	0.01, 0.0125, 0.0075 dB / mg/dl
Ref. [34]	pH of liquid sample, such as gastric acid	capacitive sensor + VCO	0.35 MHz / pH	n.a.
Ref. [35]	ϵ_r value (for saliva sample)	coplanar interdigital capacitor	129 MHz for ϵ_r from 60 to 70	n.a.
Ref. [36]	glucose concentration in fluid	liquid channel-loaded capacitor	2 MHz / mg/ml	n.a.
Ref. [37]	aqueous glucose concentration	microwave dielectric resonator	n.a.	1.2 dB from water to glucose conc. of 300 mg/ml

Ref. [38]	glucose concentration in tears	graphene-AgNW electrodes	n.a.	0.5 dB/M
Ref. [39]	glucose concentration in saliva	RF-trilayer sensor	0.6 MHz in 1 g L ⁻¹ of glucose	1 dB for saliva
Ref. [40]	pseudomonas aeruginosa, staphylococcus aureus	Interdigitated capacitor on foil	0.25 MHz per dilutions of concentration	n.a.

300

301 Thus, it can be concluded that the PHA-based LC sensor structure can successfully detect different
302 liquids to which the sensor can be exposed, through monitoring the shift in the resonant frequency. The
303 presented sensor can be calibrated using pH meter (we use pH-meter InoLab 720, WTW, Weilheim in
304 Oberbayern, Germany), bearing in mind that two studied media, saliva and gastric acid, differentiate
305 significantly in their pH values. Namely, saliva has pH value between 6.2 and 7.6, whereas gastric juice
306 has acidic pH value in the range from 1 to 2. Additionally, our measured results can be calibrated or
307 confirmed by bulky and costly HPLC or LC/MS instruments. The presented technique based on the
308 wireless principle can find useful application in the biodegradable electronics domain.

309

310 4. Conclusions

311 This work demonstrated the successful implementation of PHA as a low-cost substrate for LC resonant
312 sensors, which would increase the commercial competitiveness of these polymers. A comprehensive
313 structural, morphological and mechanical characterization of the solvent-casted mcl-PHA was
314 performed. The sensor structures were tested in air, and liquid media including artificial saliva and
315 artificial stomach acid. The sensor described in this work, realized on a biodegradable, flexible
316 substrate, can find wide application in the fields of medical diagnostics and biomedical engineering. In
317 the field of biomedicine, biopolymers show many advantages that make them superior to synthetic
318 polymers, predominantly because of their natural origin. In addition, the presented PHA sensor is
319 environmentally friendly, since there are no by-products during the fabrication process or from
320 degradation that would harm water, land, air or living things.

321

322 Acknowledgments

323 Results presented in this article received funding from the EU Horizon 2020 research and innovation
324 programme under the MSC Grant agreement no. 872370—SALSETH, and being partly supported by
325 the project 142-451-2168/2019-02, BP2017 (Bioplastech) and TR32008.

326

327 References:

- 328 [1] M. Biron, Chapter 2 – The plastics industry: economic overview. In: Biron M, editor.
329 Thermoplastics and thermoplastic composites. 3rd ed. Norwich, NY: William Andrew
330 Publishing (2018) 31–132.
- 331 [2] P.R. Rodrigues, D.J. Assis, J.I. Druzian, Simultaneous production of polyhydroxyalkanoate and
332 xanthan gum: From axenic to mixed cultivation, *Bioresource Technology* 283 (2019) 332–339.
- 333 [3] Z. Ali Raza, S. Abid, I.M. Banat, Polyhydroxyalkanoates: Characteristics, production, recent
334 developments and applications, *International Biodeterioration & Biodegradation*, 126 (2018)
335 45–56.
- 336 [4] M.E. Grigore, R.M. Grigorescu, L. Iancu, R.M. Ion, C. Zaharia, E.R. Andrei, Methods of
337 synthesis, properties and biomedical applications of polyhydroxyalkanoates: a review, *Journal*
338 *of Biomaterials Science, Polymer Edition*, (2019) DOI: 10.1080/09205063.2019.1605866.

- 339 [5] B. Hazer, A. Steinbuchel, Increased diversification of polyhydroxyalkanoates by modification
340 reactions for industrial and medical applications, *Appl Microbiol Biotechnol.* 74 (2007) 1–12.
- 341 [6] S. Ray, V.C. Kalia, Biomedical applications of polyhydroxyalkanoates, *Indian J Microbiol.* 57
342 (2017) 261–269.
- 343 [7] K. Luef, F. Stelzer, F. Wiesbrock, Poly (hydroxy alkanooate) s in medical applications. *Chem*
344 *Biochem Eng Q.* 29 (2015) 287–297.
- 345 [8] A.N. Boyandin, S.V. Prudnikova, V.A. Karpov, V.N. Ivonin, N.L. Do, T.H. Nguyen, T.M.H.
346 Le, N.L. Filichev, A.L. Levin, M.L. Filipenko, T.G. Volova, I.I. Gitelson, Microbial
347 degradation of polyhydroxyalkanoates in tropical soils. *Int. Biodeterior. Biodegr.* 83 (2013) 77–
348 84.
- 349 [9] A. Larrañaga, J. Fernández, A. Vega, A. Etzeberria, C. Ronchel, J.L. Adrio, J.R. Sarasua,
350 Crystallization and its effect on the mechanical properties of a medium chain length
351 polyhydroxyalkanoate, *J. Mech. Behav. Biomed. Mater.* 39 (2014) 87–94.
- 352 [10] S. Philip, T. Keshavarz, I. Roy, Polyhydroxyalkanoates: biodegradable polymers with a range
353 of applications, *J. Chem. Technol. Biotechnol.* 82 (2007) 233–247.
- 354 [11] K. Jia, R. Cao, D. Hua, P. Li, Study of class I and class III polyhydroxyalkanoate (PHA)
355 synthases with substrates containing a modified side chain, *Biomacromolecules* 17 (4) (2016)
356 1477–1485.
- 357 [12] A. Anjum, M. Zuber, K. Zia, A. Noreen, M. Anjum, S. Tabasum, Microbial production of
358 polyhydroxyalkanoates (PHAs) and its copolymers: a review of recent advancements, *Int. J.*
359 *Biol. Macromol.* 89 (2016) 161–174.
- 360 [13] V. Urtuvia, P. Villegas, S. Fuentes, M. González, M. Seeger, *Burkholderia xenovorans* LB400
361 possesses a functional polyhydroxyalkanoate anabolic pathway encoded by the pha genes and
362 synthesizes poly(3-hydroxybutyrate) under nitrogen-limiting conditions, *Int. Microbiol.* 21 (1–
363 2) (2018) 47–57.
- 364 [14] E. Bugnicourt, P. Cinelli, A. Lazzeri, V. Alvarez, Polyhydroxyalkanoate (PHA): review of
365 synthesis, characteristics, processing and potential applications in packaging. *Express Polym.*
366 *Lett.* 8, (2014) 791–808.
- 367 [15] C. Sanhueza, F. Acevedo, S. Rocha, P. Villegas, M. Seeger, R. Navia, Polyhydroxyalkanoates
368 as biomaterial for electrospun scaffolds, *International Journal of Biological Macromolecules*
369 124 (2019) 102–110.
- 370 [16] Z.A. Raza, S. Riaz, I.M. Banat, Polyhydroxyalkanoates: properties and chemical modification
371 approaches for their functionalization. *Biotechnol Progress.* 34 (2018) 29–41.
- 372 [17] L. Gong, D.B. Chase, I. Noda, J. Liu, D.C. Martin, C. Ni, J.F. Rabolt, Discovery of β -form
373 crystal structure in electrospun poly[(R)-3-hydroxybutyrate-co-(R)-3-hydroxyhexanoate]
374 (PHBHx) nanofibers: from fiber mats to single fibers, *Macromolecules* 48 (17) (2015) 6197–
375 6205.
- 376 [18] D. Kim, H. Kim, M. Chung, Y. Rhee, Biosynthesis, modification, and biodegradation of
377 bacterial medium-chain-length polyhydroxyalkanoates, *J. Microbiol.* 45 (2) (2007) 87–97.
- 378 [19] T. Volova, D. Goncharov, A. Sukovaty, A. Shabanov, E. Nikolaeva, E. Shishatskaya,
379 Electrospinning of polyhydroxyalkanoate fibrous scaffolds: effects on electrospinning
380 parameters on structure and properties, *J. Biomater. Sci. Polym. Ed.* 25 (4) (2014) 370–393.
- 381 [20] M. Zhu, W. Zuo, H. Yu, W. Yang, Y. Chen, Superhydrophobic surface directly created by
382 electrospinning based on hydrophilic material, *J. Mater. Sci.* 41 (12) (2006) 3793–3797.
- 383 [21] M. Xiang, L. Xinjian, X. Han, L. Genxi, Direct electrochemistry and electrocatalysis of
384 hemoglobin in poly-3-hydroxybutyrate membrane, *Biosensors and Bioelectronics*, 20 (9)
385 (2005) 1836–1842.
- 386 [22] X. Ma, R. Yang, G. Li, Hydrogen Peroxide Biosensor Based on the Direct Electrochemistry of
387 Myoglobin Immobilized in Poly-3-Hydroxybutyrate Film, *Am. J. Biochem. Biotechnol.* 1
388 (2005) 43–46.

- 389 [23] P. Phukon, K. Radhapyari, B. K. Konwar, R. Khan, Natural polyhydroxyalkanoate–gold
390 nanocomposite based biosensor for detection of antimalarial drug artemisinin, *Materials*
391 *Science and Engineering: C*, 37 (2014) 314–320.
- 392 [24] R. Davis, G. Duane, S.T. Kenny, F. Cerrone, M.W. Guzik, R.P. Babu, E. Casey, K.E.
393 O’Connor, High cell density cultivation of *Pseudomonas putida* KT2440 using glucose without
394 the need for oxygen enriched air supply, *Biotechnol. Bioeng.* 112 (4) (2015) 725–733.
- 395 [25] Y. Elbahloul, A. Steinbüchel, Large-scale production of poly(3-hydroxyoctanoic acid) by
396 *Pseudomonas putida* GPo1 and a simplified downstream process. *Appl. Environ. Microbiol.* 75
397 (3) (2009) 643–651.
- 398 [26] X. Pan, J. Li, R. Gun, X. Hu, Preparation and in Vitro Evaluation of Enteric-coated Tablets of
399 Rosiglitazone sodium. *Saudi Pharmaceutical Journal* 23 (2015) 581–586.
- 400 [27] A. Rodriguez-Contreras, Recent Advances in the Use of Polyhydroxyalkanoates in Biomedicine;
401 *Bioengineering*, 6 (2019) 82.
- 402 [28] J. Limb, M. You, J. Li, Z. Li, Emerging bone tissue engineering via Polyhydroxyalkanoate
403 (PHA)-based scaffolds, *Materials Science and Engineering: C*, 79 (2017) 917–929.
- 404 [29] B.Y. Yu, C.R. Chen, Y.M. Sun, T.H. Young, The response of rat cerebellar granule neurons
405 (rCGNs) to various polyhydroxyalkanoate (PHA) films, *Desalination* 245 (2009) 639–646
- 406 [30] K. Sofinska, J. Barbasz, T. Witko, J. Dryzek, K. Harażna, M. Witko, J. Krysiak-Czerwenka,
407 M. Guzik, Structural, topographical, and mechanical characteristics of purified
408 polyhydroxyoctanoate polymer, *J. Appl. Polym. Sci.* 2019.
- 409 [31] A. Benken, Y. Gianchandani, Passive Wireless Pressure Sensing for Gastric Manometry,
410 *Micromachines* 10 (2019), 868–646.
- 411 [32] S. Saremi-Yarahmadi, O. H. Murphy, C. Toumazou, RF Inductive Sensors for Detection of
412 Change in the Ionic Strength and pH of Liquid Samples, *Proc. of 2010 IEEE International*
413 *Symposium on Circuits and Systems*, 30 May-2 June 2010, Paris, France, doi:
414 10.1109/ISCAS.2010.5536953.
- 415 [33] M. Dautta, M. Alshetaiwi, J. Escobar, P. Tseng, Passive and wireless, implantable glucose
416 sensing with phenylboronic acid hydrogel-interlayer RF resonators, *Biosensors and*
417 *Bioelectronics* 151 (2020) 112004.
- 418 [34] M.S. Arefin, M.B. Coskun, T. Alan, J.M. Redoute, A. Neild, M.R. Yuce, A microfabricated
419 fringing field capacitive pH sensor with an integrated readout circuit, *Appl. Phys. Lett.* 104,
420 (2014) 223503.
- 421 [35] G. Crupi, X. Bao, O. J. Babarinde, D. M. M.-P. Schreurs, B. Nauwelaers, Biosensor using a
422 one-port interdigital capacitor: A resonance-based investigation of the permittivity sensitivity
423 for microfluidic broadband bioelectronics applications, *Electronics*, 9 (2020), 340
- 424 [36] N. K. Tiwari, S. P. Singh, D. Mondal, M. Jaleel Akhtar, Flexible biomedical RF sensors to
425 quantify the purity of medical grade glycerol and glucose concentrations, *International Journal*
426 *of Microwave and Wireless Technologies* (2019) 1–11.
- 427 [37] S. Kim, J. Kim, A. Babajanyan, K. Lee, B. Friedman, Noncontact characterization of glucose
428 by a waveguide microwave probe, *Current Applied Physics* 9 (2009) 856–860.
- 429 [38] J. Kim, M. Kim, M. S. Lee, K. Kim, S. Ji, Y. T. Kim, J. Park, K. Na, K. H. Bae, H. K. Kim, F.
430 Bien, C. Y. Lee, J. U. Park, Wearable smart sensor systems integrated on soft contact lenses for
431 wireless ocular diagnostics, *Nature communication*, 8 (2016) 14997.
- 432 [39] P. Tseng, B. Napier, L. Garbarini, D. L. Kaplan, F. G. Omenetto, Functional, RF-Trilayer
433 Sensors for Tooth-Mounted, Wireless Monitoring of the Oral Cavity and Food Consumption,
434 *Adv. Mater.* (2018), 1703257.
- 435 [40] T. Kojić, M. Radovanović, G. Stojanović, B. Pivaš, D. Medić, H. Al-Salami, Comparison of
436 performances of flexible sensors on foil and paper for efficient bacterial concentration
437 measurement, *Sensor Review*, 40 (2020) 1–7.

439
440
441
442
443
444
445
446
447
448
449
450
451
452
453
454
455
456
457
458
459
460
461
462
463
464
465
466
467
468
469
470
471
472

Figure captions:

Figure 1. (a) Visual appearance of the processed PHA sample, (b) SEM micrograph of the sample at $\times 200$ magnification, (c) SEM micrograph of the sample cross-section at $\times 250$ magnification

Figure 2. (a) 2D profilometer image of surface structure of sample; (b) 3D profilometer image of sample

Figure 3. Three-dimensional AFM images of PHA sample topography obtained for two scanning areas: (a) $50\ \mu\text{m} \times 50\ \mu\text{m}$ and (b) $5\ \mu\text{m} \times 5\ \mu\text{m}$

Figure 4. 2D AFM images showing topography ((a) and (c)) and LFM signal ((b) and (d)) for the scanned areas $50\ \mu\text{m} \times 50\ \mu\text{m}$ and $5\ \mu\text{m} \times 5\ \mu\text{m}$

Figure 5. (a) Detail of the user interface of ImageJ software during the measurement of the contact angle (b) Graphical representation of contact angle results for a drop of distilled water

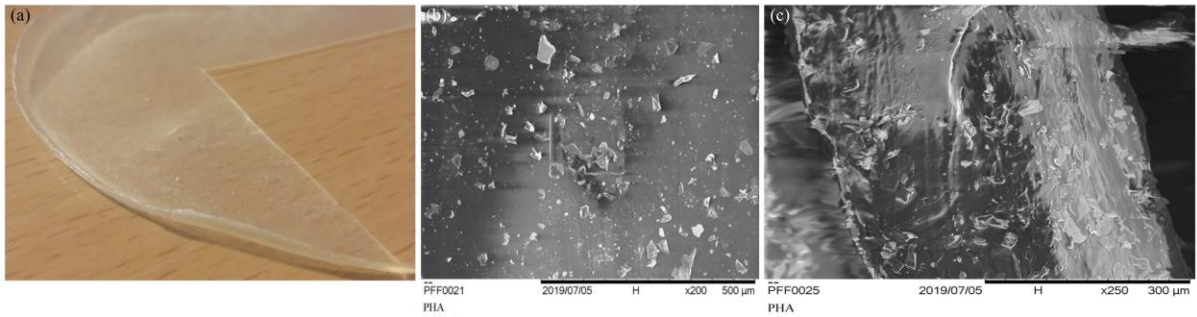
Figure 6. Load-displacement curves for three analyzed cases

Figure 7. LC resonant structure: (a) manufactured from PHA, (b) after gold coating

Figure 8. Sensor appearance when there is artificial saliva between the capacitor electrodes

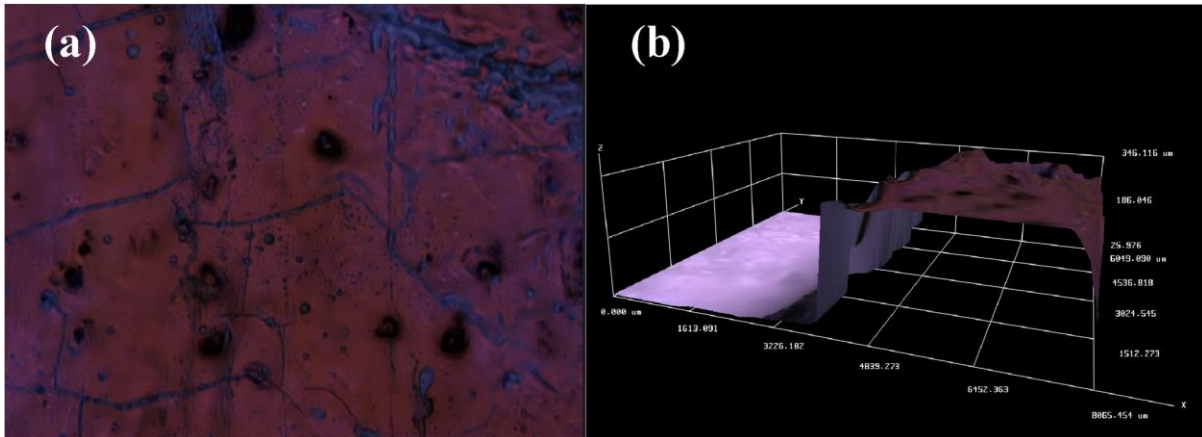
Figure 9. Frequency dependence of amplitude of S11 parameters in three chosen media

Figure 10. Variation of the resonant frequency depending on the type of the medium



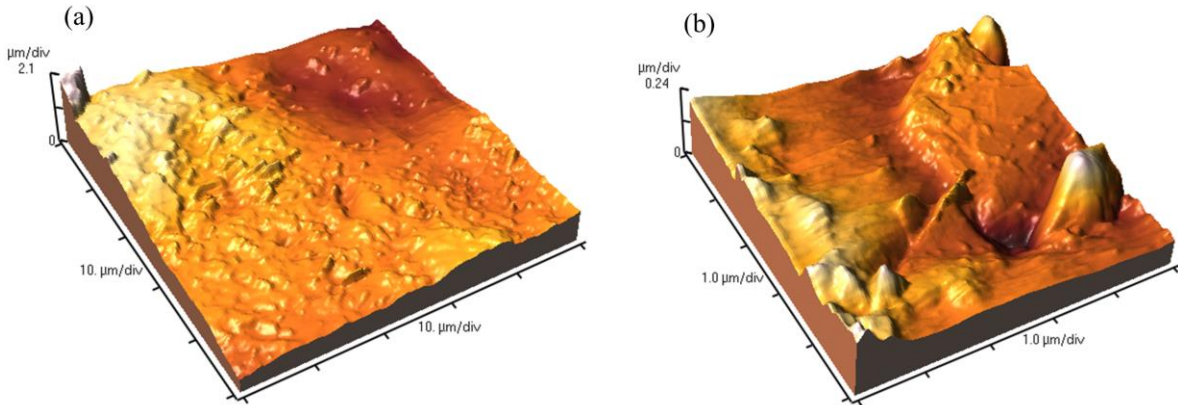
473

474



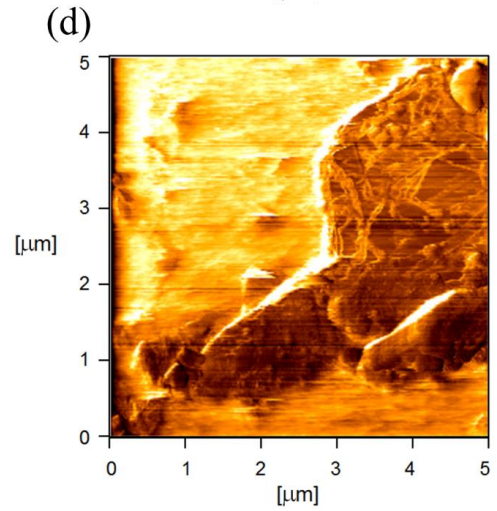
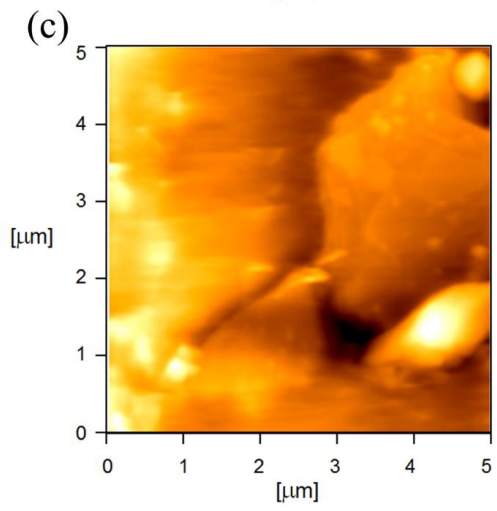
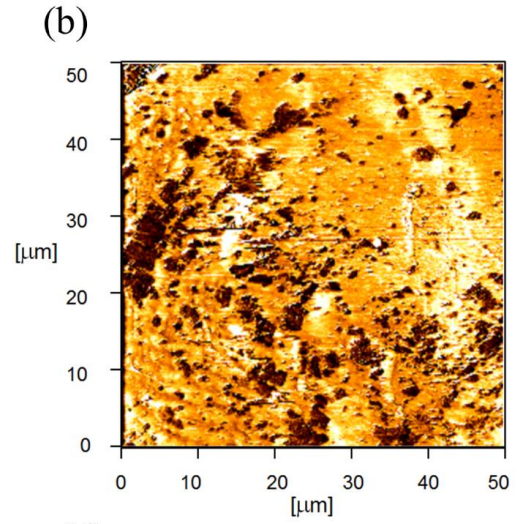
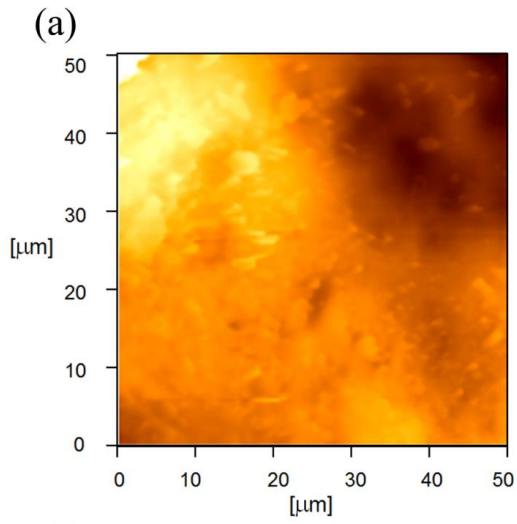
475

476

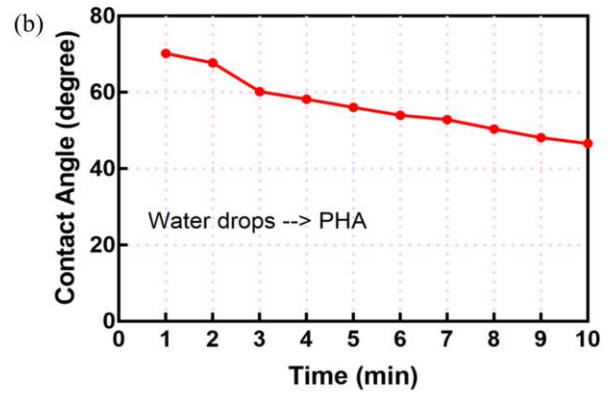
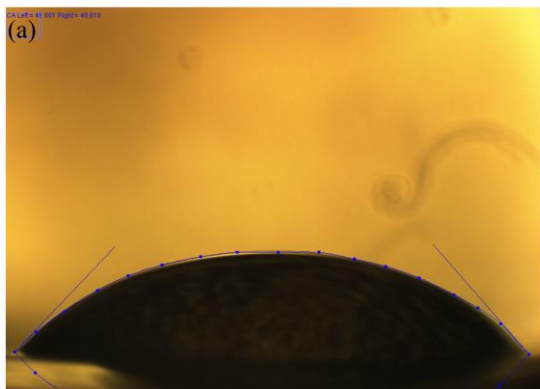


477

478

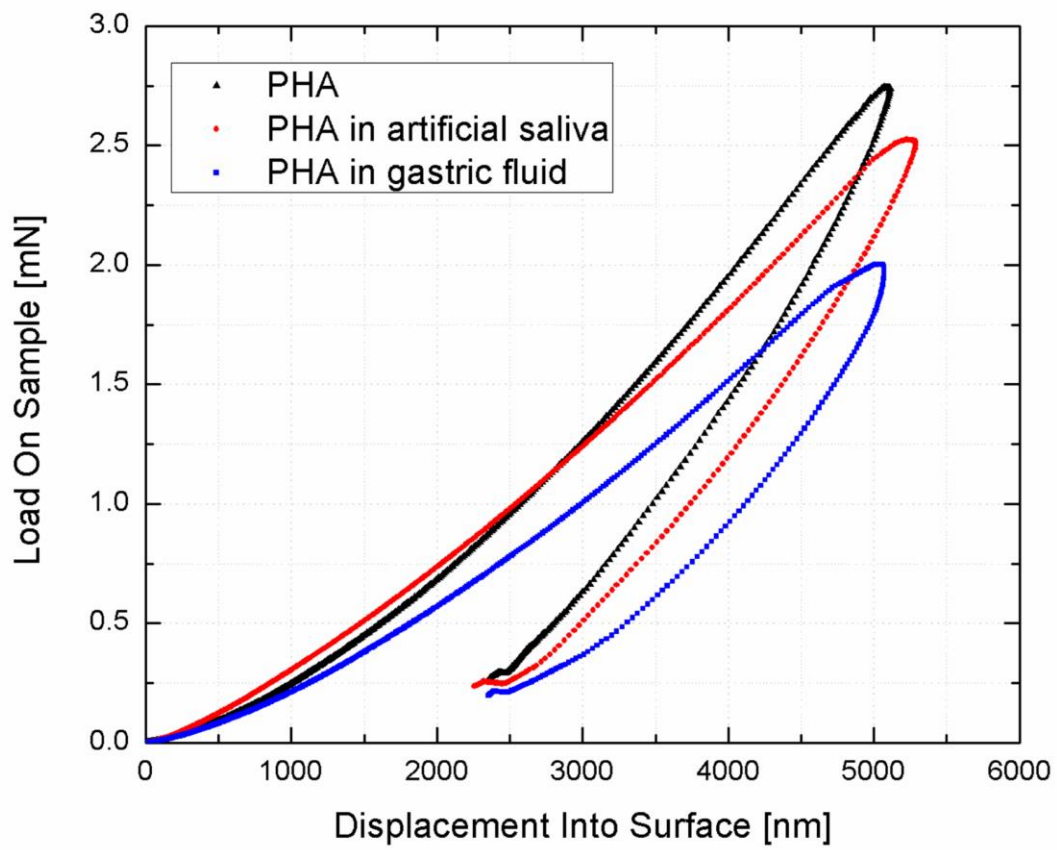


479

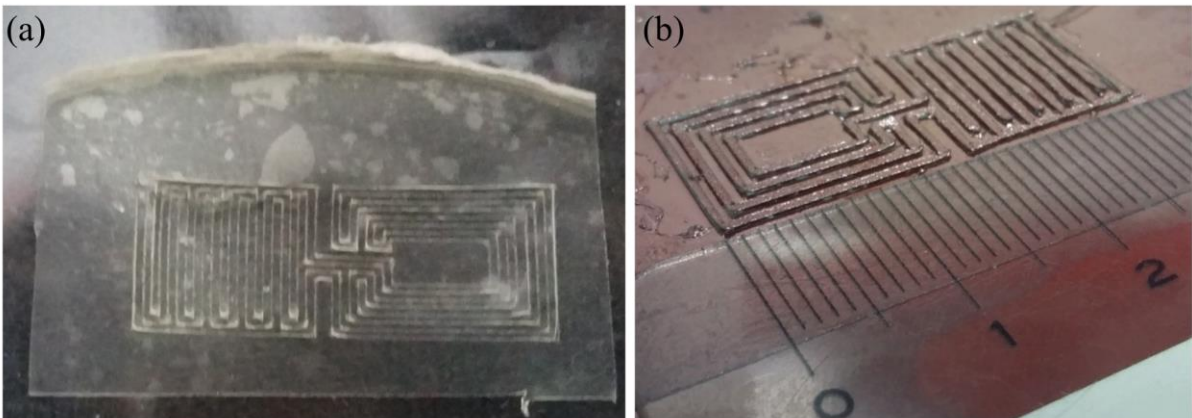


480

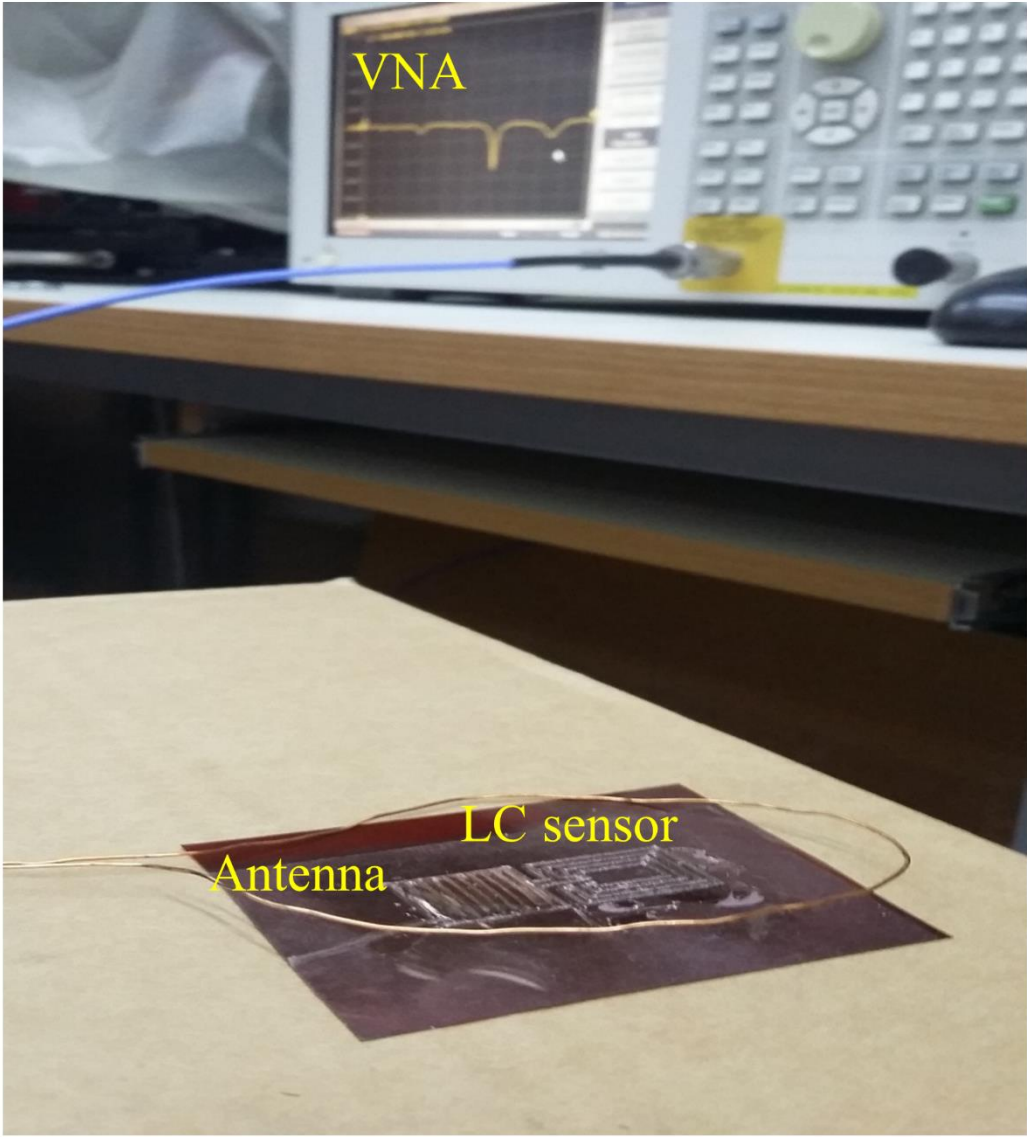
481

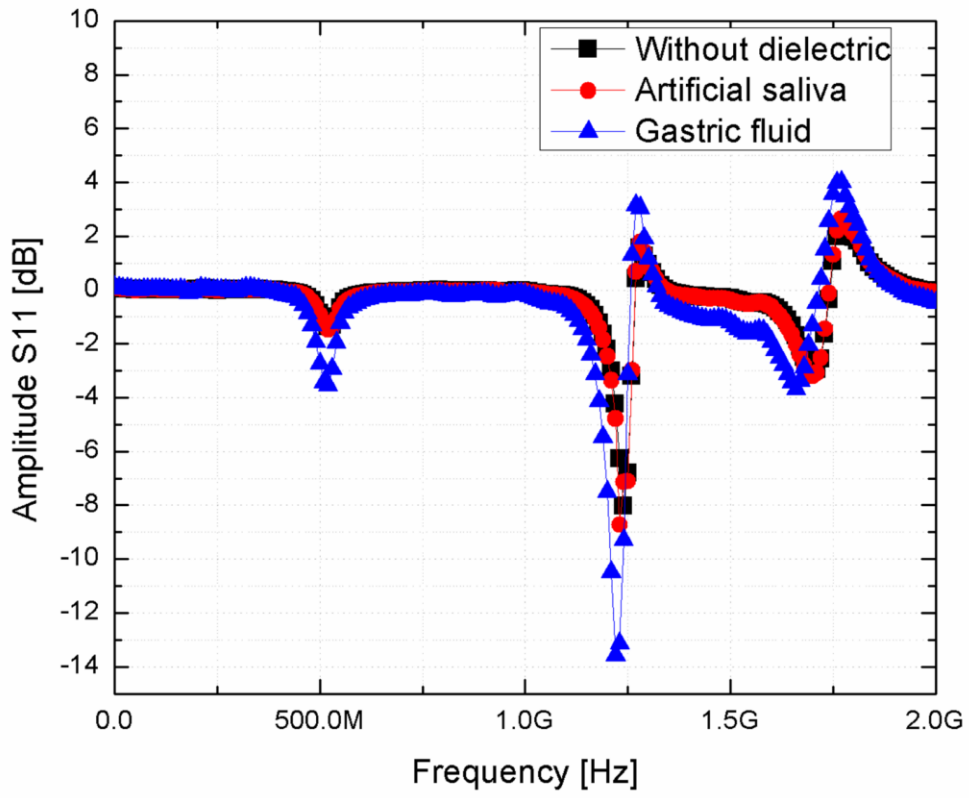


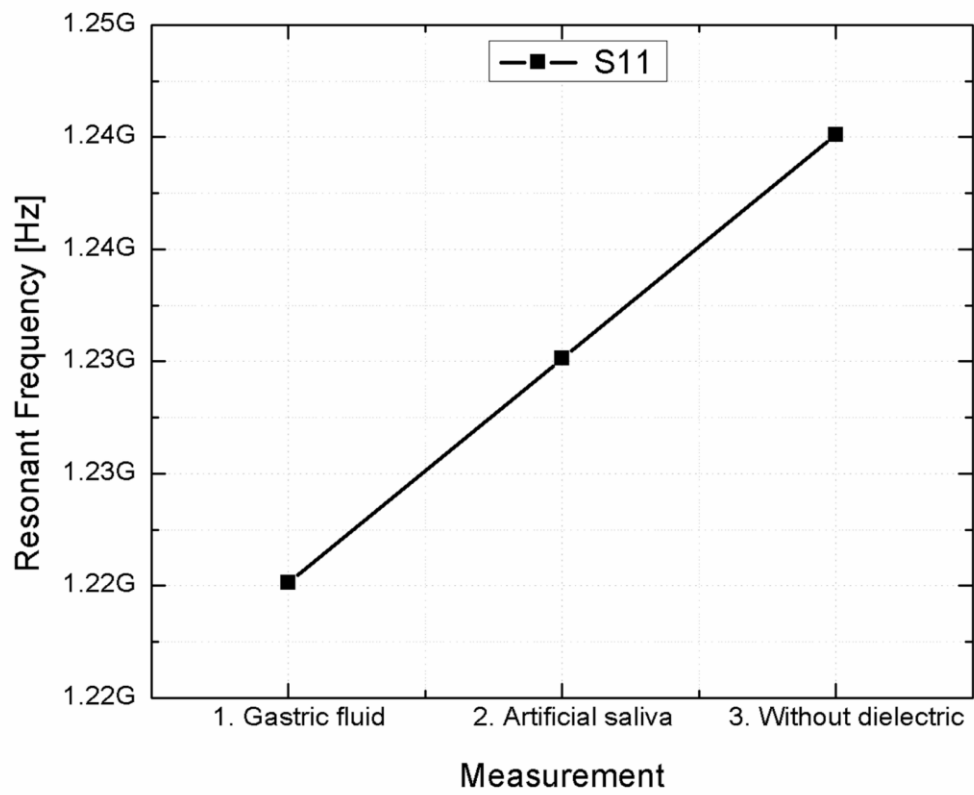
482



483







486

487